Article:
Blain, T., Basta, G., Taylor-Mew, J. et al. (2026) Planar InAs avalanche photodiodes with high gain and low noise factor. Optics Express, 34 (8). pp. 14623-14631. ISSN: 1094-4087

https://doi.org/10.1364/oe.592771

Research Article Vol. 34, No. 8 / 20 Apr 2026 / Optics Express 14623
Optics EXPRESS

Planar InAs avalanche photodiodes with high gain and low noise factor

T. Blain, G. Basta, J. Taylor-Mew, I. S. Han, M. Hopkinson, J. P. R. David, J. S. Ng, and C. H. Tan*

School of Electrical and Electronic Engineering, University of Sheffield, South Yorkshire, UK
*c.h.tan@sheffield.ac.uk

Abstract: In photon-starved extended short- and mid-wave infrared optical applications, replacing Mercury Cadmium Telluride (HgCdTe) avalanche photodiodes (APDs) with Indium Arsenide (InAs) APDs offers significant environmental and cost benefits. To demonstrate InAs APDs as a viable alternative, we fabricated planar devices using ion implantation and rigorously characterised multiple devices under high-gain operating conditions. These planar APDs exhibited a very low excess noise factor ($F \sim 1.4$) for gains up to 250 at 77 K, comparable to HgCdTe devices. We believe this to be the first experimental report of such low excess noise in planar InAs APDs, marking a significant step towards establishing them as a realistic alternative.

1. Introduction

There is a wide range of optical applications operating in extended shortwave- and mid-wave-infrared (eSWIR and MWIR) bands. Examples include atmospheric gas sensing [1], radiation thermometry [2], and LiDAR [3]. In optical receivers of such systems, semiconductor photodiodes or avalanche photodiodes (APDs) not only perform an essential function (converting optical signals into an electrical signal), but often also determine the optical receivers' signal-to-noise ratio (SNR). Given that these optical applications are usually photon-starved, a high-performance APD with (i) high quantum efficiency, QE, (ii) high avalanche multiplication, *M,* at minimal excess noise factors, *F,* and (iii) low dark current is often used (instead of a photodiode) in the receiver to improve its SNR.

$Hg_{1-x}Cd_xTe$ APDs are established options for photon-starved optical applications in the eSWIR and MWIR bands, because those with Cd compositions < 0.6 have high *M* with a minimal *F*, owing to the multiplication process solely dominated by electrons [4]. For example, when operated at 80 K, $Hg_{0.7}Cd_{0.3}Te$ APDs with a cutoff-wavelength λ_c, = 4.4 µm (QE > 80% up to 4.0 µm) produced *M* up to ~1100 with $F < 2$ [5]. An HgCdTe APD with a $\lambda c = 4.3$ µm has been reported with a Noise Equivalent Power (NEP) of 0.5 $fW.Hz^{-0.5}$ [6]. However, increasing the Cd composition leads to lower avalanche gain at a given APD bias voltage, e.g. *M* ~100 for $\lambda_c = 3.9$ µm materials cf. $M \sim 8$ for $\lambda_c = 2.5$ µm materials at a bias of 8 V [7]. One significant drawback is that most $Hg_{1-x}Cd_xTe$ APDs (with $x < 0.6$) require cryogenic operating temperature (e.g. 80 [5] and 120 K [6]) to suppress the APDs' dark currents associated with the small bandgap of $Hg_{1-x}Cd_xTe$. Furthermore, a global environmental agreement (in force since 2017) aims to reduce the use of mercury [8], directly affecting $Hg_{1-x}Cd_xTe$ APDs. Hence, mercury-free alternatives for eSWIR and MWIR APDs are needed.

As part of the efforts to find such alternatives as well as the general pursuit for avalanche materials with low excess noise performance, compound III-V Separate-Absorption-Multiplication APDs (SAM APDs) have been developed. They utilized two Sb-based alloys, $Al_xIn_{1-x}AsSb$

#592771 https://doi.org/10.1364/OE.592771
Journal © 2026 Received 4 Feb 2026; revised 23 Mar 2026; accepted 24 Mar 2026; published 9 Apr 2026

Optics EXPRESS

and $Al_xGa_{1-x}AsSb$, which exhibit low excess noise characteristics and are promising avalanche materials. Grown lattice matched to a GaSb substrate, an $Al_{0.3}In_{0.7}AsSb$ absorption layer ($\lambda_c = 2.1$ µm) was combined with an $Al_{0.7}In_{0.3}AsSb$ avalanche layer to achieve $F \sim 2$ at $M = 10$ [9]. Reducing the Al composition in $Al_xIn_{1-x}AsSb$ can extend λ_c, but the excess noise characteristics worsen, such as the $Al_{0.05}InAsSb$ APD with $\lambda_c \sim 3.5$ µm where $F \sim 2$ at $M = 5$ [10]. $Al_{0.85}Ga_{0.15}As_{0.56}Sb_{0.44}$, lattice matched to InP substrates, also exhibits very low excess noise with $F < 2$ for $M < 25$ [11]. A SAM APD combining $Al_{0.85}Ga_{0.15}As_{0.56}Sb_{0.44}$ avalanche region with InGaAs-GaAsSb Type II superlattice absorber achieved $\lambda_c \sim 2.4$ µm and $F < 2$ for $M < 20$ [12]. Another SAM APD consisted of an $Al_{0.9}Ga_{0.1}As_{0.08}Sb_{0.92}$ avalanche region and an InGaAsSb absorber (grown on GaSb substrates), which achieved a $\lambda_c \sim 2.75$ µm at room temperature and $F = 4.5$ at $M = 20$ [13]. Overall, although these Sb-based SAM APDs achieved low F for $M < 50$, they fail to match the excess noise performance and high QE at wavelengths above 3 µm offered by $Hg_{1-x}Cd_xTe$ APDs.

InAs APDs are suitable for the eSWIR and MWIR bands. InAs exhibits an external QE of 48% (without anti-reflection coating) at the peak wavelength of 3.35 µm [2]. Experimental reports have established that InAs exhibits electron-only multiplication [14,15], with $F < 2$, which is independent of M and temperature [16]. To date, InAs is therefore the only compound III-V semiconductor with excess noise and QE performance approaching those of $Hg_{1-x}Cd_xTe$. What makes InAs an interesting alternative to HgCdTe for MWIR is that, unlike HgCdTe, it can be grown on a cheaper native substrate, and the active avalanche region is a simple binary InAs with no issue related to alloy composition uniformity. Commercial interest in InAs APD has also increased as its epitaxial growth is now available in the foundry to support applications such as gas sensing [17].

The maximum M of previously reported InAs APDs is limited by either band-to-band tunnelling and/or surface leakage currents. In earlier InAs APDs (mesa devices with 2 - 3.5 µm unintentional doped InAs avalanche regions and background doping density $\sim 1 \times 10^{15}$ cm^{-3}), tunnelling currents limited the maximum M to < 10 at room temperature [13,14]. This value was later improved to 80, owing to a thicker avalanche region (~ 6 µm) with a lower background doping density (7×10^{14} cm^{-3}) [18]. Reducing the background doping further yielded higher M [19] and was successfully demonstrated in InAs mesa APDs. To suppress surface leakage currents, planar InAs APDs were subsequently developed, involving optimization of ion implantation and thermal annealing conditions for epitaxially grown InAs wafers [20,21]. These resulted in a 128-pixel linear array of planar InAs APD exhibiting good pixel-to-pixel uniformity of avalanche gain and responsivity at room temperature and 200 K [22]. Planar InAs APDs have achieved M as high as 330 (at 200 K), achieved with a background doping ~2×14 cm^{-3} [23]. However, there is a lack of $F(M)$ data from planar InAs APDs [20,21,22,24], with all existing InAs $F(M)$ data from mesa InAs APDs [13,14,15,17,18]. Even in mesa InAs APDs, there is no $F(M)$ data beyond $M > 30$. These gaps hinder progress in technological maturity and adoption of InAs APDs, which are promising alternative to HgCdTe APDs in photon-starved eSWIR and MWIR optical applications.

In this work, we report the first experimental $F(M)$ characteristics from planar InAs APDs, with $F < 2$ at M upto 250 and exhibiting a Noise Equivalent Power (NEP) of 22 fW·Hz$^{-0.5}$. They detected 1550 nm wavelength optical signal as weak as 16 photons per 50 µs pulse, demonstrating low photon detection capability.

2. Experimental details

InAs epilayers were grown by molecular beam epitaxy (MBE) on 2" (100) vertical temperature gradient freeze (VGF) substrates at 480 °C. The structure consisted of a 100 nm n^+ InAs layer (Si-doped 1×10^{18} cm^{-3}), followed by a 500 nm InAs n-layer (Si-doped 5×10^{17} cm^{-3}) and a 9.4 µm intrinsic InAs layer. Device fabrication processes yielded planar devices with sizes of

Optics EXPRESS

80×80, 200×200, and 400×400 μm^2, as illustrated in Fig. 1. The p$^+$ - InAs regions were formed by selective area Beryllium (Be) ion implantation with an implant energy of 45 keV and a dose of 2.3×10^{14} cm^{-2}. The conditions were chosen to yield a Be implant profile with a depth of 300 - 400 nm, as shown in Fig. 1(a). The profile was simulated using the Transport of Ions in Matter software [25]. The ion implantation was followed by rapid-thermal-annealing at 550 °C for 30 seconds. Top and back (substrate side) Ti/Au contacts were deposited by sputtering. SU-8 passivation covered the active area partially and Ti/Au bondpads to the devices were deposited on Si_3N_4.

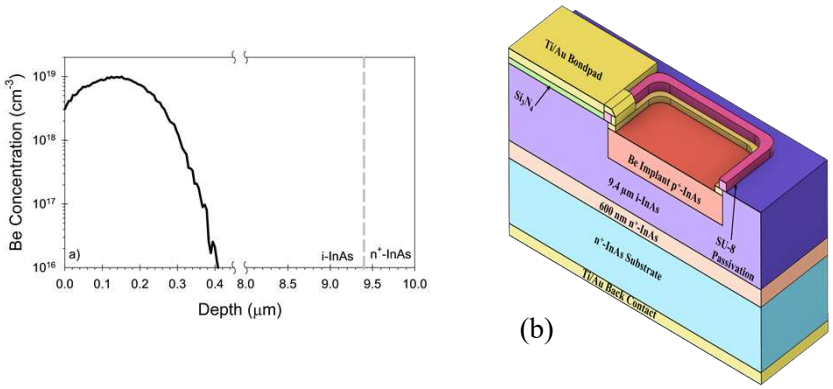

Fig. 1. (a) Simulated Be implant profile (solid line) into the intrinsic InAs layer, with a dashed line indicating the i-n junction at 9.4 μm. (b) Schematic of a planar InAs p-i-n APD.

Electrical and optical characterization were performed on 200×200 and 400×400 μm^2 APDs, using three APDs from each size (labelled A, B, and C). The devices were placed inside a liquid-nitrogen-cooled probe station equipped with a heater stage to control the device temperature, as shown in Fig. 2(a). Dark and photocurrent measurements (at 1550 nm wavelength) for device-under-test (DUT) were performed using a source-measure unit, which simultaneously provided reverse bias to the DUT and measured current flowing through the DUT. Capacitance-Voltage, *C-V*, measurements over a reverse bias range from 0 to -17 V were performed with the DUT at 77 K (to limit the influence of dark current on the measurement) using an LCR meter (not shown in Fig. 2(a)). The doping profile of the InAs APDs was extracted assuming single-sided depletion and a relative dielectric constant of 15.15 for InAs [26]. Characteristics of avalanche gain versus reverse bias, $M(V)$, was obtained by measuring the DUT's current with the DUT being illuminated by a continuous-wave 1550 nm wavelength laser. From the experimental photocurrent data, we obtained $M(V) = \frac{I_{total}(V) - I_d(V)}{I_{pri}}$, where I_{total} is the total current under light illumination, I_d is the dark current, and I_{pri} is the primary photocurrent when $M = 1$. The extracted photocurrent values, $I_{ph}(V) = I_{total}(V) - I_d(V)$, remain constant with reverse bias between 0 and 0.6 V, as shown in Fig. 2(b). Hence, the mean value of I_{ph} in that bias range was used for I_{pri}. Also, between 0 and -10 V, experimental values of I_{total} were around an order of magnitude higher than those of I_d at 200 K and ~3 orders at 77 K.

$F(M)$ measurements at 1550 nm wavelength were carried out using a similar approach to [27,28], under the illumination of the continuous-wave laser in Fig. 2(a) on the largest devices (400 μm × 400 μm) to ensure light was confined to the DUT's active area. Different optical power levels (12, 2.5, and 0.56 μW) were used to check that the $F(M)$ data were independent of optical power. In the setup, the DUT's current was amplified by a low-noise current pre-amplifier. The amplified signal was fed to a Fast-Fourier-Transform spectrum analyzer to measure its power spectral density (PSD). Measurement frequency range was set as 12 - 18 kHz, avoiding 1/f

Optics EXPRESS

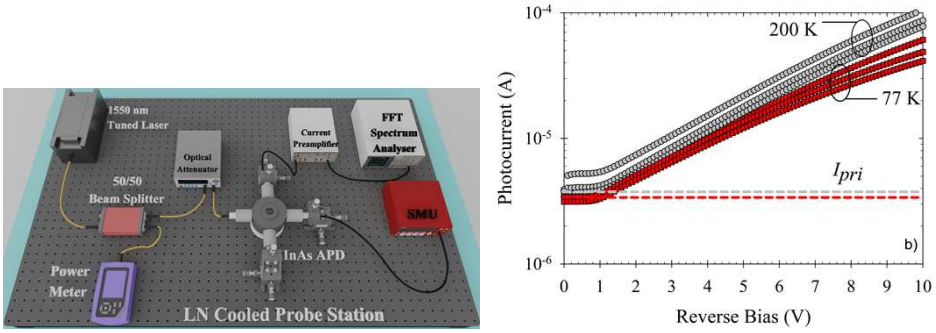

Fig. 2. (a) Experimental setup. (b) Experimental photocurrent versus reverse bias characteristics at 77 and 200 K from three 200×200 μm^2 APDs.

noise while remaining within the frequency range of the pre-amplifier. Measurements of PSD were repeated with DUT in the dark or under laser illumination, yielding $\mathrm{PSD_{dark}}$ and $\mathrm{PSD_{total}}$, respectively. The excess noise factor is given by $F = \frac{PSD_{total} - PSD_{dark}}{2qI_{ph}MB}$, where q is the elementary charge of an electron, and B is the measurement bandwidth (6 kHz). $2qI_{ph}MB$ is the total ideal shot noise associated with the DUT's current when under illumination. Values of NEP were given by $\mathrm{NEP} = \frac{\text{Measured Noise}}{M \times \text{Responsivity}}$ and utilized the smaller $80\,\mu\mathrm{m} \times 80\,\mu\mathrm{m}$ APDs to minimize the dark current.

3. Results and discussion

Doping profiles extracted from the 77 K *C-V* data of a total of six APDs are in agreement, as shown in Fig. 3. As reverse bias increases, the depletion width increases, eventually reaching 9 μm. This is close to the intended depletion width, considering the Be implant depth of ~ 400 nm in a 9.4 μm (as grown) undoped InAs layer. The level of unintentional doping density is very low at $\sim 1.4 \times 10^{14}\,\mathrm{cm^{-3}}$. The combination of low unintentional doping density and the relatively thick as-grown i-InAs layer has led to an improvement (increase) in depletion width compared to previous InAs APDs (depletion width of 6 - 8 μm [17,22,23]). This is desirable for increasing the maximum M of InAs APDs.

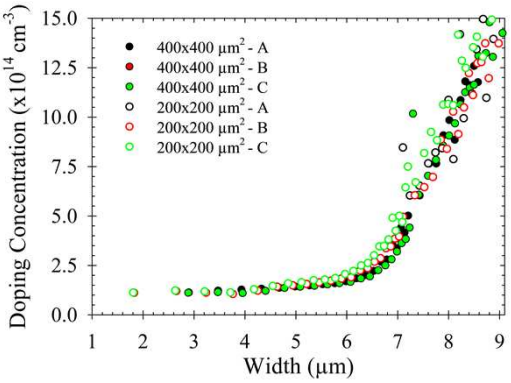

Fig. 3. Doping profiles obtained from six InAs APDs, using C-V data measured at 77 K.

Dark current data from three 200×200 μm^2 APDs at 200 and 77 K are shown in Fig. 4(a). The associated photocurrent data are shown earlier in Fig. 2(b). For a given temperature, dark

Optics EXPRESS

current and photocurrent data from different APDs agree. As the temperature decreases from 200 to 77 K, the dark current decreases by three orders of magnitude, with the photocurrents higher than the dark currents over the voltage range used. Avalanche gain data from these APDs for a given temperature (200 and 77 K) are also in agreement, as shown in Fig. 4(b). At 200 K, M ~ 300 was obtained at - 23 V, while $M > 200$ at 77 K was obtained at – 30 V. These high gains were possible because there is a large depletion width in our APDs and $M = \exp(\alpha w)$ in InAs. However, the gain increases more gradually at high bias. This is due to an initial rapid increase in w that produces a rapid increase in αw. Once the avalanche region is fully depleted, the gain increases more slowly as α has a relatively weak dependence on electric field in InAs [15]. For a given reverse bias, values of M at 77 K are lower than those at 200 K, which is consistent with previous reports (e.g. [15], [18]) and is attributed to α decreasing with decreasing temperature in InAs [18].

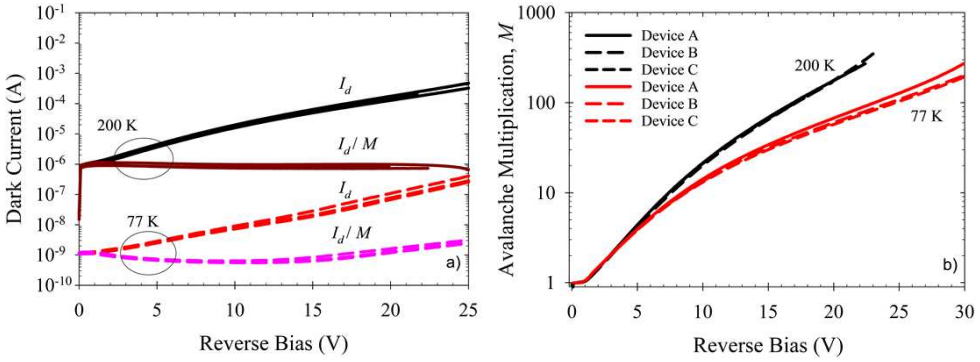

Fig. 4. (a) Dark current and gain-normalized dark current, and (b) avalanche gain versus reverse bias from three 200 × 200 μm^2 APDs

Characteristics of gain-normalized dark currents, I_d/M, versus reverse bias at 200 K are also shown in Fig. 4(a). I_d/M is constant at 200 K, indicating that the dark current and the 1550 nm wavelength photocurrent (resulting from electrons generated by photon absorption in the p$^+$-InAs region) experience similar avalanche gain. This in turn indicates two desirable attributes: (i) the dark current at 200 K is dominated by diffusion current, and (ii) tunnelling currents are negligible compared to the diffusion current in these InAs APDs. The dominance of diffusion current at temperatures ≥ 200 K is consistent with characteristics of previous planar InAs APDs [23]. The negligible tunnelling current can be attributed to relatively low electric fields, facilitated by the low unintentional doping density and the wide depletion region in these APDs. At 77 K, values of I_d/M vary slightly with reverse bias, with a minima at ~ - 12 V. Between 0 and 1 V, values of I_d/M are slightly higher than the experimental value of I_d. The discrepancy suggests the presence of surface-related dark current that does not experience M. For biases above -12 V, values of I_d/M increase with reverse bias gradually, which may be attributed to the increasing prominence of dark current mechanisms such as band-to-band or trap-assisted tunnelling current. A more detailed investigation of the dark current characteristics at 77 K would require further temperature dependence measurements, which are outside the scope of this work.

Experimental noise power spectral densities versus frequency with the APDs (400 × 400 μm^2) at different applied biases in the dark and when illuminated with the 1550 nm laser at 77 K are shown in Fig. 5(a) and (b), respectively. The reverse bias of the APD were varied from 0 to 32.5 V, and the optical power used was 12 μW. For a given reverse bias, PSD_{dark} readings are constant with frequency, indicating that the readings are dominated by the amplifier's noise. As reverse bias increases, the PSD_{dark} data exhibit a step increase from -20 to - 22 V, due to a reduction in

Optics EXPRESS

the amplifier's noise (associated with reduced amplifier's gain from 100 to 50 kV/A). For a given reverse bias, values of PSD_{dark} is lower than values of $PSD_{total,}$ the noise power spectral densities due to photocurrent, shown in Fig. 5(c), can be extracted using the subtraction method.

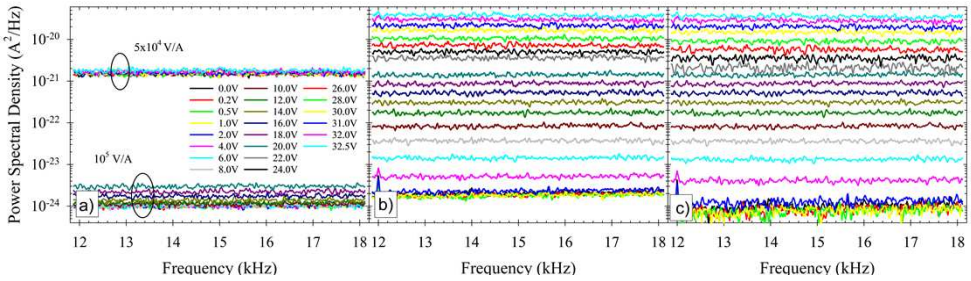

Fig. 5. Power Spectral Density the from a $400 \times 400\ \mu m^2$ APD when (a) in the dark, and (b) illuminated with 1550 nm wavelength laser. (c) Extracted power spectral density from photocurrent at 77 K.

Data from Fig. 5(c) are replotted as characteristics of the photocurrent PSD versus photocurrent in Fig. 6(a). These are in agreement with data from two other DUTs (obtained using optical powers of 0.56 and 2.5 μW), also shown in Fig. 6(a), confirming the validity of our experimental results. For a given photocurrent, the experimental PSD value is significantly higher than $2qI$ (shot noise without avalanche gain) and marginally higher than $2qIM$ (shot noise multiplied by experimental values of M). $F(M)$ characteristics extracted from these PSD data are compared in Fig. 6(b). The planar InAs APDs exhibit $F \sim 1.4$ for M up to 250 at 77 K, consistent with mesa InAs APD reports (which are more limited in the range of M) and established impact ionization theory for InAs ($F = 1.5$ - 1.6) [14,15]. Since the $F(M)$ characteristics in mesa InAs APDs exhibit a relatively weak temperature dependence [15], the $F(M)$ characteristics of InAs planar APDs are not expected to change significantly with temperature.

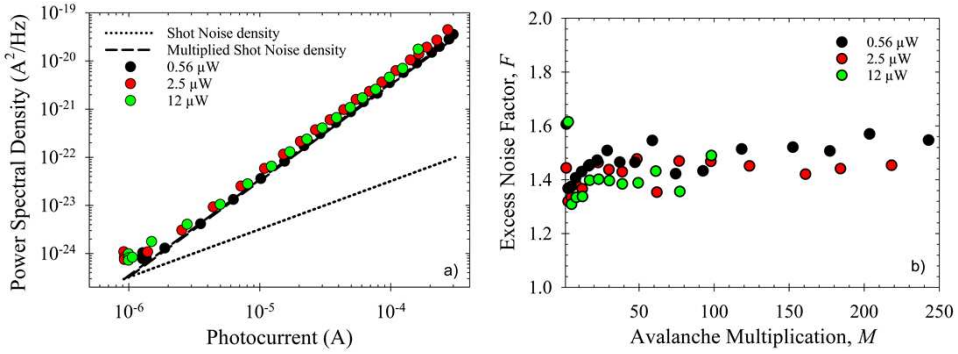

Fig. 6. (a) Photocurrent PSD vs photocurrent and (b) Excess noise factor vs avalanche gain characteristics of the InAs APDs ($400 \times 400\ \mu m^2$) at 77 K measured using optical power of 0.56, 2.5 and 12 μW.

Figure 7 compares the $F(M)$ characteristics of this work with those published for an $Hg_{0.6}Cd_{0.4}Te$ APD [29], an $InGaAs/Al_{0.85}Ga_{0.15}As_{0.56}Sb_{0.44}$ APD (on InP substrate) [30], and a Type II Superlattice $(InGaAs\text{-}GaAsSb)/Al_{0.85}Ga_{0.15}As_{0.56}Sb_{0.44}$ APD (on InP substrate) [11]. The InAs planar APD and the $Hg_{0.6}Cd_{0.4}Te$ APDs have similar cutoff wavelength, and their $F(M)$ characteristics are similar (the best in this comparison). The $InGaAs/Al_{0.85}Ga_{0.15}As_{0.56}Sb_{0.44}$

Optics EXPRESS

APD is among the lowest excess noise APDs for 1550 nm wavelength operation (with a shorter cutoff wavelength than InAs and $Hg_{0.6}Cd_{0.4}Te$). Its excess noise factors are significantly higher than those of InAs, because $Al_{0.85}Ga_{0.15}As_{0.56}Sb_{0.44}$ does not exhibit electron-only multiplication. Experimental report of $F(M)$ characteristics for eSWIR APD with a Type II absorber is limited to $M < 30$ and indicates worse performance than the other APDs in Fig. 7.

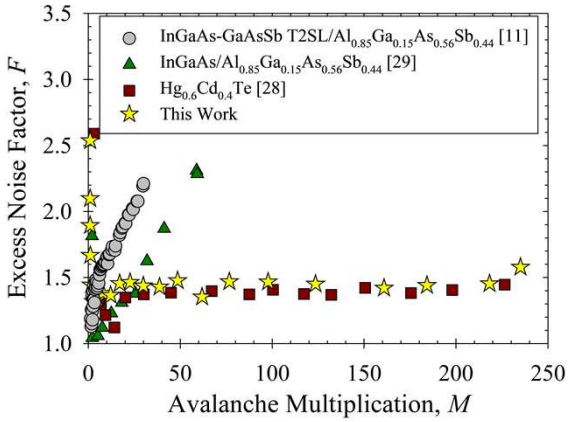

Fig. 7. Excess noise factor vs avalanche gain comparison between this work and select SWIR $Hg_{0.6}Cd_{0.4}Te$ [28], and $Al_{0.85}Ga_{0.15}As_{0.56}Sb_{0.44}$ [11,29], and this work.

The characteristics for the NEP versus M of the InAs planar APDs at 77 K are shown in Fig. 8(a). They exhibit a minimum (best) value of 22 fW·Hz$^{-0.5}$ at $M = 100$ (reverse bias of -27 V), after which NEP increases due to the onset of tunnelling current, as indicated by the gain-normalized dark current in Fig. 4(a). The best NEP value from this work is half of the 45 fW·Hz$^{-0.5}$ from Ref. [23]. There is potential to improve the NEP value from 22 to 13 fW·Hz$^{-0.5}$, by optimizing the APD anti-reflection coating (not performed in work). The unity gain responsivity of the APDs of this work at 1550 nm is 0.6 A/W, corresponding to an external quantum efficiency of 48%. Increasing the APD's external quantum efficiency to 80% (routinely achieved in InGaAs photodiodes with anti-relection coatings) would reduce the NEP value to 13 fW·Hz$^{-0.5}$, making InAs APDs an attractive option for low photon sensing at wavelengths beyond the operating range of InGaAs photodiodes, such as MWIR gas sensing. While the NEP of the InAs APDs is presently higher than that of the HgCdTe [R.1], InAs APDs have a far simpler epitaxial growth process compared to HgCdTe, and the NEP can be further reduced with a reduction in the dark current of the APDs, either by improving crystal growth, reducing the physical diameter or improving the quality of the devices. For example, a commercial InAs photodiode [31] exhibit a room temperature dark current density of 46 mA.cm^{-2} compared to 1 A.cm^{-2} in our current devices suggesting further improvement can be achieved.

To demonstrate the low photon detection capability, we used a pulse laser and attenuated the power with a calibrated variable optical fiber attenuator. The laser was pulsed at ~10 kHz, with a 50:50 duty cycle. The number of photons illuminating the sample surface was determined by measuring the optical power of the laser on the sample stage and attenuating it to 16 photons using a calibrated fiber-coupled variable optical attenuator. Figure 8(b) shows that a clearly detectable peak was obtained when the APD was biased at -27 V and illuminated with an average photon number of 16 photons per laser pulse (50 µs). This is 4 times lower than the 70 photons per pulse detection achieved in the previous work [23].

Optics EXPRESS

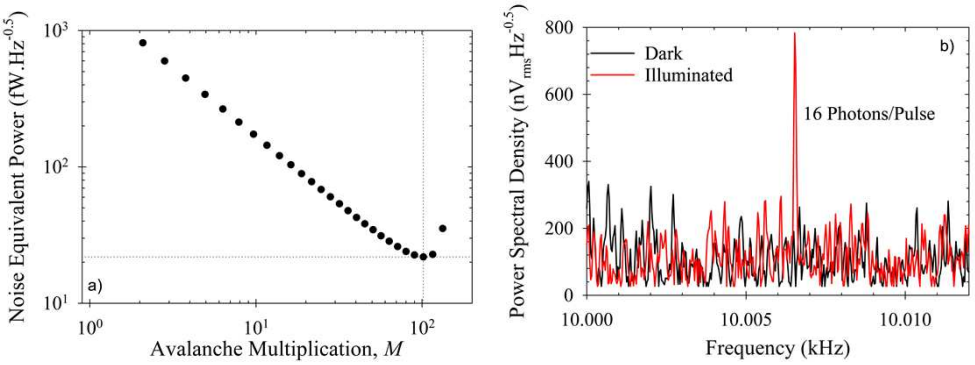

Fig. 8. (a) Noise equivalent power of an 80×80 μm^2 pixel measured at 77 K. (b) Power spectral density at 27 V in the dark and with 16 photons per pulse, measured at 77 K.

4. Conclusion

Planar InAs APDs of varying active areas have been fabricated using Be ion implantation. The planar APDs repeatedly achieved avalanche gains > 300 at 200 K (200 at 77 K). Experimental $F(M)$ data (the first report from InAs planar APDs) show $F \sim 1.4$ for M values up to 250 at 77 K, in line with existing reports from mesa InAs APDs (which are more limited in the range of M) as well as established impact ionization theory for this material ($F = 1.5$ - 1.6). Their $F(M)$ data are also comparable to those of $Hg_{0.6}Cd_{0.4}Te$ APDs, the current detectors of choice for photo-starved eSIWR and MWIR optical applications but are incompatible with global efforts to reduce mercury usage.

Our experimental minimum (best) value for NEP of these InAs APDs is 22 fW·Hz$^{-0.5}$, when operated at avalanche gain of 100 and cooled to 77 K. Onset of tunnelling current is currently limiting further increase in the operating gain (and hence reduction in NEP). Nevertheless, our APDs could detect 1550 nm wavelength optical signals as weak as 16 photons/pulse. Our results represent a significant increase in the technological maturity of InAs APDs, making them a realistic alternative to HgCdTe APDs in eSWIR and MWIR optical applications.

Funding. Engineering and Physical Sciences Research Council (EP/S026428/1).

Disclosures. The authors declare no conflicts of interest.

Data availability. Data underlying the results presented in this paper are available at ORDA digital repository [32].

References

1. U. N. Singh, T. F. Refaat, M. Petros, *et al.*, "Evaluation of 2- μ m Pulsed Integrated Path Differential Absorption Lidar for Carbon Dioxide Measurement—Technology Developments, Measurements, and Path to Space," IEEE J. Sel. Top. Appl. Earth Observations Remote Sensing **11**(6), 2059–2067 (2018).
2. X. Zhou, X. Meng, A. B. Krysa, *et al.*, "InAs Photodiodes for 3.43 μm Radiation Thermometry," IEEE Sensors J. **15**(10), 5555–5560 (2015).
3. R. H. Hadfield, J. Leach, F. Fleming, *et al.*, "Single-photon detection for long-range imaging and sensing," Optica **10**(9), 1124 (2023).
4. A. Singh, V. Srivastav, and R. Pal, "HgCdTe avalanche photodiodes: A review," Opt. Laser Technol. **43**(7), 1358–1370 (2011).
5. P. D. Anderson, J. D. Beck, W. Sullivan, *et al.*, "Recent Advancements in HgCdTe APDs for Space Applications," J. Electron. Mater. **51**(12), 6803–6814 (2022).
6. X. Sun, J. B. Abshire, J. D. Beck, *et al.*, "HgCdTe avalanche photodiode detectors for airborne and spaceborne lidar at infrared wavelengths," Opt. Express **25**(14), 16589 (2017).
7. P. Thorne and C. Turner, "Progress at Leonardo UK in APD array technology development for high-speed 2D linear mode photon-counting applications," in *Infrared Technology and Applications* L. D. Z. Ting, G. F. Fulop, M. Kimata, and M. H. MacDougal, eds., National Harbor, United States: SPIE, June 2024, p. 8.
8. M. A. Coulter, "Minamata Convention on Mercury," Int. leg. mater. **55**(3), 582–616 (2016).

Optics EXPRESS

9. A. H. Jones, S. D. March, S. R. Bank, *et al.*, "Low-noise high-temperature AlInAsSb/GaSb avalanche photodiodes for 2-μm applications," Nat. Photonics **14**(9), 559–563 (2020).
10. A. A. Dadey, J. A. McArthur, A. Kamboj, *et al.*, "High-gain low-excess-noise MWIR detection with a 3.5- μ m cutoff AlInAsSb-based separate absorption, charge, and multiplication avalanche photodiode," APL Photonics **8**(3), 036101 (2023).
11. J. Taylor-Mew, V. Shulyak, B. White, *et al.*, "Low Excess Noise of Al 0.85 Ga 0.15 As 0.56 Sb 0.44 Avalanche Photodiode From Pure Electron Injection," IEEE Photonics Technol. Lett. **33**(20), 1155–1158 (2021).
12. H. Jung, S. Lee, X. Jin, *et al.*, "Low excess noise and high quantum efficiency avalanche photodiodes for beyond 2 μm wavelength detection," Commun Mater **5**(1), 219 (2024).
13. X. Jin, S. Zhao, A. P. Craig, *et al.*, "High-performance room temperature 2.75 μm cutoff In0.22 Ga0.78 As0.19 Sb0.81 /Al0.9 Ga0.1 As0.08 Sb0.92 avalanche photodiode," Optica **11**(12), 1632 (2024).
14. A. R. J. Marshall, C. H. Tan, M. J. Steer, *et al.*, "Electron dominated impact ionization and avalanche gain characteristics in InAs photodiodes," Appl. Phys. Lett. **93**(11), 111107 (2008).
15. A. R. J. Marshall, Chee Hing Tan, M. J. Steer, *et al.*, "Extremely Low Excess Noise in InAs Electron Avalanche Photodiodes," IEEE Photonics Technol. Lett. **21**(13), 866–868 (2009).
16. P. J. Ker, J. P. R. David, and C. H. Tan, "Temperature dependence of gain and excess noise in InAs electron avalanche photodiodes," Opt. Express **20**(28), 29568 (2012).
17. website, "InAs Electron Avalanche Photodiode (e-APD) Epiwafer *S," XIAMEN POWERWAY. Accessed: Nov. 18, 2025. [Online]. Available: https://www.powerwaywafer.com/electron-avalanche-photodiode-epi.html
18. S. J. Maddox, W. Sun, Z. Lu, *et al.*, "Enhanced low-noise gain from InAs avalanche photodiodes with reduced dark current and background doping," Appl. Phys. Lett. **101**(15), 151124 (2012).
19. W. Sun, Z. Lu, X. Zheng, *et al.*, "High-Gain InAs Avalanche Photodiodes," IEEE J. Quantum Electronics **49**(2), 154–161 (2013).
20. B. S. White, I. C. Sandall, J. P. R. David, *et al.*, "InAs Diodes Fabricated Using Be Ion Implantation," IEEE Trans. Electron Devices **62**(9), 2928–2932 (2015).
21. L. W. Lim, C. H. Tan, J. S. Ng, *et al.*, "Improved Planar InAs Avalanche Photodiodes With Reduced Dark Current and Increased Responsivity," J. Lightwave Technol. **37**(10), 2375–2379 (2019).
22. T. Osman, L. W. Lim, J. S. Ng, *et al.*, "Fabrication of infrared linear arrays of InAs planar avalanche photodiodes," Opt. Express **30**(12), 21758–21763 (2022).
23. B. S. White, I. C. Sandall, X. Zhou, *et al.*, "High-Gain InAs Planar Avalanche Photodiodes," J. Lightwave Technol. **34**(11), 2639–2644 (2016).
24. T. Blain, V. Shulyak, I. S. Han, *et al.*, "Low Noise Equivalent Power InAs Avalanche Photodiodes for Infrared Few-Photon Detection," IEEE Trans. Electron Devices **71**(5), 3039–3044 (2024).
25. J. F. Ziegler, M. D. Ziegler, and J. P. Biersack, "SRIM – The stopping and range of ions in matter (2010)," Nuclear Instruments and Methods in Physics Research Section B: Beam Interactions with Materials and Atoms **268**(11-12), 1818–1823 (2010).
26. M. V. Fischetti, "Monte Carlo simulation of transport in technologically significant semiconductors of the diamond and zinc-blende structures. I. Homogeneous transport," IEEE Trans. Electron Devices **38**(3), 634–649 (1991).
27. A. Karar, R. Tanaka, and J. Ch. Vanel, "APD's excess noise measurements using spectral analysis (FFT)," Nuclear Instruments and Methods in Physics Research Section A: Accelerators, Spectrometers, Detectors and Associated Equipment **387**(1-2), 205–210 (1997).
28. A. A. Dadey, J. A. McArthur, A. H. Jones, *et al.*, "Considerations for excess noise measurements of low-k-factor Sb-based avalanche photodiodes," J. Opt. Soc. Am. A **40**(6), 1225 (2023).
29. Z. Wang, L. Zhu, Z. Yang, *et al.*, "Low excess noise HgCdTe e-SWIR avalanche photodiode operating at high gain and temperature," Infrared Phys. Technol. **141**, 105419 (2024).
30. B. Sheridan, X. Collins, J. Taylor-Mew, *et al.*, "An Extremely Low Noise-Equivalent Power Photoreceiver Using High-Gain InGaAs/AlGaAsSb APDs," J. Lightwave Technol. **43**(2), 741–746 (2025).
31. Laser Components, "InAs Photodiode IA35-Series," Accessed: Apr. 28, 2022. [Online]. Available: https://www.lasercomponents.com/fileadmin/user_upload/home/Datasheets/lc-ingaas/ia35s500-inas.pdf
32. ORDA digital repository, "InGaAs/AlGaAsSb avalanche photodiode with high gain-bandwidth product,"